Cell. Mol. Life Sci. (2015) 72:1417–1432
DOI 10.1007/s00018-014-1761-6

Cellular and Molecular Life Sciences

RESEARCH ARTICLE

Directed structural modification of *Clostridium perfringens* enterotoxin to enhance binding to claudin-5

Jonas Protze · Miriam Eichner · Anna Piontek · Stefan Dinter · Jan Rossa · Kinga Grażyna Blecharz · Peter Vajkoczy · Joerg Piontek · Gerd Krause

Received: 24 April 2014 / Revised: 8 October 2014 / Accepted: 13 October 2014 / Published online: 24 October 2014

Abstract *Clostridium perfringens* enterotoxin (CPE) binds to distinct claudins (Clds), which regulate paracellular barrier functions in endo- and epithelia. The C-terminal domain (cCPE) has the potential for selective claudin modulation, since it only binds to a subset of claudins, e.g., Cld3 and Cld4 (cCPE receptors). Cld5 (non-CPE receptor) is a main constituent in tight junctions (TJ) of the blood-brain barrier. We aimed to reveal claudin recognition mechanisms of cCPE and to create a basis for a Cld5-binder. By utilizing structure-based interaction models, mutagenesis and assays of cCPE-binding to the TJ-free cell line HEK293, transfected with human Cld1 and murine Cld5, we showed how cCPE-binding to Cld1 and Cld5 is prevented by two residues in extracellular loop 2 of Cld1 (Asn^{150} and Thr^{153}) and Cld5 (Asp^{149} and Thr^{151}). Binding to Cld5 is especially attenuated by the lack of a bulky hydrophobic residue like leucine at position 151. By downsizing the binding pocket and compensating for the lack of this leucine residue, we created a novel cCPE-variant; $cCPE_{Y306W/S313H}$ binds Cld5 with nanomolar affinity (K_d 33 ± 10 nM). Finally, the effective binding to endogenously Cld5-expressing blood-brain barrier model cells (murine microvascular endothelial cEND cell line) suggests $cCPE_{Y306W/S313H}$ as basis for Cld5-specific modulation to improve paracellular drug delivery, or to target claudin overexpressing tumors.

Keywords Tight junctions · Protein–protein interactions · Membrane proteins · Drug delivery system · Structure–function study · Mutagenesis · Molecular modeling

Abbreviations

TJ	Tight junctions
CPE	*Clostridium perfringens* Enterotoxin
cCPE	C-terminal domain of *Clostridium perfringens* enterotoxin
Cld	Claudin
ECL	Extracellular loop
PDB	Protein data bank
RMSD	Root mean square deviation

Introduction

Claudins which form the backbone of tight junctions (TJ) are expressed in a tissue-specific manner and regulate paracellular permeability in endo- and epithelia [1, 2]. The mammalian claudin family comprises at least 26 different subtypes, which are tetraspan transmembrane domain proteins. Most, if not all, claudin subtypes form polymers by both *cis*-interactions (with claudins within the same cell

J. Piontek and G. Krause contributed equally to this work.

Electronic supplementary material The online version of this article (doi:10.1007/s00018-014-1761-6) contains supplementary material, which is available to authorized users.

J. Protze · M. Eichner · A. Piontek · S. Dinter · J. Rossa · G. Krause (✉)
Leibniz-Institut für Molekulare Pharmakologie, Robert-Rössle-Str. 10, 13125 Berlin, Germany
e-mail: GKrause@fmp-berlin.de

K. G. Blecharz · P. Vajkoczy
Department of Neurosurgery, Charité-Universitätsmedizin Berlin, 13353 Berlin, Germany

J. Piontek
Institute of Clinical Physiology, Charité-Universitätsmedizin Berlin, 12203 Berlin, Germany

membrane) and *trans*-interactions (with claudins of the neighboring cell membrane). Just recently a crystal structure of claudin-15 (Cld15) comprising the four transmembrane helices and the extra- and intracellular loops (PDB ID:4P79, [3]) was released, nevertheless the molecular mechanisms of claudin–claudin interactions are still unclear. However, nature has provided us with a protein that can be used as a molecular tool. *Clostridium perfringens* enterotoxin (CPE) binds to claudin-3 (Cld3) and claudin-4 (Cld4) [4], which were first reported as CPE receptors [5]. CPE can be used to elucidate mechanistic details of claudin's extracellular interactions and to target claudins for modulation of the barrier function. CPE also binds to several similar members of the claudin family—the "CPE receptors" [6], but not to other claudins such as Cld2 and Cld5 ("non-CPE receptors"). Cld1 was initially reported to be a non-CPE receptor [7], but it was later shown that CPE does interact with Cld1, albeit weakly [8, 9]. The crystal structure of CPE comprises three domains [10, 11]. The C-terminal domain of CPE contains the claudin-binding site [12], which consists of a deep and strongly hydrophobic pit formed by three tyrosines (Tyr^{306}, Tyr^{310} and Tyr^{312}; triple-Tyr pit) and a shallower and less hydrophobic/non-polar pit framed by three leucines (Leu^{225}; Leu^{254}; Leu^{315}) [9]. The two N-terminal domains of CPE cause cytotoxicity by mediating pore formation in the plasma membrane of the host mucosa cells, leading to cell death [13, 14]; whereas the C-terminal domain of CPE (cCPE) on its own is non-cytotoxic [15, 16]. However, since cCPE binds to extracellular loop 2 (ECL2) of distinct claudins [6], it increases paracellular permeability for ions and solutes by affecting the TJ reversibly [7] and was thus suggested to be a promising selective modulator of claudins [15, 16]. cCPE enhances drug absorption in the rat jejunum [17] and was shown to be effective in mucosal vaccination [18, 19]. Furthermore, since tumor proliferation and growth are associated with deregulation of claudin subtype expression and function [20], CPE constructs can be used to target tumors that overexpress claudin [21–24] and labeled cCPE was successfully used to detect Cld4-overexpressing cancer cells in vivo [25]. Unlike other drug absorption enhancers like chitosan and sodium caprate [26–28], cCPE acts specifically on its receptors; however, the determinants of this specificity are still unclear. Moreover, claudin subtype-specific binders are not yet available. We and others demonstrated that the claudin-binding properties of cCPE can be selectively changed by multiple mutations in cCPE [9, 29]. After we showed that Cld3 and Cld4 interact with cCPE by different mode of actions, we were able to create cCPE-variants binding predominantly either to Cld3 or Cld4. In addition, we showed that the contact between a bulky hydrophobic residue (Leu^{150} in Cld3 and Leu/Met^{151} in Cld4) and the triple-Tyr pit of CPE is one of the key interactions in cCPE–claudin binding [9].

In this study, we analyzed the cCPE–claudin interaction in more detail (I) to understand the binding mechanism and (II) to lay a foundation for the development of cCPE as a claudin subtype-specific *biological* for tissue-specific TJ- and claudin modulation. We aimed to identify the molecular features that underlie the strong interaction between cCPE and Cld3 and Cld4, the weak interaction with Cld1 and the lack of an interaction with Cld5. Cld5 is a non-CPE receptor. However, since it is responsible for sealing the blood–brain barrier, our main aim was to develop a cCPE-variant with enhanced specificity for Cld5, as this might allow the modulation of even a non-CPE receptor claudin. Using a rational molecular and structure-based approach, we studied the mechanisms of interaction between cCPE and the ECL2 of Cld1, Cld3 and Cld5 at the level of individual residues. With this approach, it was possible to deduce information about the structural properties of the ECL2 of these claudins. On the basis of these molecular insights, we were able to change individual amino acid residues in cCPE in such a way that a cCPE-variant was produced with nanomolar affinity to Cld5. We proved the concept that directed modifications of cCPE allow a targeted interaction with distinct claudin subtypes, even with non-CPE receptor claudins. These findings open the way to specific pharmacological interventions to improve tissue-specific paracellular drug delivery or tumor treatment.

Materials and methods

Plasmids

For the construction of plasmid encoding GST-$CPE_{194\text{-}319}$ (GST-cCPE) fusion protein, cDNA of CPE (kindly provided by Dr. Y. Horiguchi, Osaka, Japan) was amplified by PCR and cloned into pGEX-4T1 (GE Healthcare, Munich, Germany), using EcoRI and SalI [30]. Plasmids encoding GST-$CPE_{194\text{-}319}$ with single or multiple mutations (L238F, I258 K, V259Y, A302 M, A302Y, S305P, Y306A Y306 W, S307R, Y310H, Y310K, S313H, L315A) were generated by site-directed mutagenesis of pGEX-4T1-$CPE_{194\text{-}319}$, as described earlier [30]. Plasmids based on pEYFP-N1 encoding murine $Cld3_{WT}$-YFP [30], murine $Cld5_{WT}$-YFP [31], $Cld5_{R145Q}$, $Cld5_{E146A}$-YFP [32], human $Cld1_{WT}$-YFP [33], $Cld5_{D149N}$, $Cld5_{T151L}$, $Cld5_{D149N/T151L}$-YFP, ChF, $ChF_{D148N/T150L}$-YFP and ChG-YFP [34] have been described previously. $Cld1_{D150N}$, $Cld1_{T153V}$, $Cld1_{D150N/T153V}$-YFP and $ChG_{D148N/T150L}$-YFP were generated by site-directed mutagenesis of $Cld1_{WT}$-YFP or ChG-YFP, respectively. pEGFP-Cld4 encoding human Cld4 with N-terminal GFP was kindly provided by Dr.

W. Hunziker (Singapore). Murine Cld6, −7, −8 and −9 were obtained from OriGene Technologies, Inc. (Rockville, MD, USA) and plasmids originating from pEYFP-N1 encoding Cld6, −7, −8 and −9-YFP were generated by restriction-free cloning [35].

Antibodies

Phycolink® anti-GST R-phycoerythrin-conjugated antibodies (Europa Bioproducts Ltd, Cambridge, UK), goat HRP-anti-mouse (Invitrogen, Carlsbad, USA), mouse anti-GST (Sigma-Aldrich, Steinheim, Germany) and mouse anti-GFP/YFP (Clonetech Mountain View, USA).

Expression and purification of cCPE-constructs

$CPE_{194\text{-}319}$ with N-terminal GST fusions as well as GST (control) was expressed in E. coli BL21. Bacteria were grown to A600 = 0.6–0.8, expression induced by addition of 1 mM isopropyl-β-D-thiogalactopyranoside. 3 h after induction, bacteria were harvested (10 min, 20.000×*g*, 4 °C) and lysed in PBS (phosphate buffered saline) with 1 % (v/v) Triton X-100, 0.1 mM PMSF, 1 mM EDTA, protease inhibitor cocktail (Sigma-Aldrich, Steinheim, Germany) and sonicated with Vibra Cell™ Model 72434 (BioBlock Scientific, Strasbourg, France) by 10 × 1 s pulses. Insoluble cell debris was removed by centrifugation (20,000×*g* for 1 h at 4 °C). Proteins were purified from supernatants using glutathione-agarose (Sigma-Aldrich, Steinheim, Germany) and dialyzed against PBS. Protein concentration was determined with BCA Protein Kit (Thermo-Scientific, Rockford, USA).

Labeling of GST-cCPE

Labeling of GST-cCPE with AlexaFluor®647 was performed utilizing the AlexaKit (Invitrogen) and GST-$cCPE_{K257A}$. This mutant interacts similarly to $cCPE_{WT}$ with all claudins tested so far and was used to prevent inhibition of binding to claudins by coupling the amino-reactive fluorophore to Lys^{257}—which is in close vicinity to the claudin-binding pocket of cCPE. The resulting Alexa647–cCPE showed a labeling of 9 mol AlexaFluor®647 per mol GST-$cCPE_{K257A}$.

Cell culture and transfection

HEK293 cell cultivation, transient or stable transfection, as well as selection of stable HEK293 cell lines expressing murine Cld6-, Cld7-, Cld8- or Cld9-YFP were performed as described [32].

cEND cells were maintained as described [36]. For experimental setups, cEND cells were allowed to reach 80 % confluence and incubated in serum reduced DMEM with 2 % (v/v) of dextran-coated charcoal-treated FCS (Fetal calf serum) for 24 h.

Live cell imaging

For live cell imaging, the transfected cells were transferred to 1 ml DMEM, 10 mM N-(2-hydroxyethyl)piperazine-N'(2-ethane- sulfonic acid) pH 7.5 without phenol red. For cCPE-binding, cells were incubated with 2 µg/ml Alexa647-cCPE. To study subcellular localization of claudin-variants, the plasma membrane was visualized by addition of 20 µl trypan blue, 0.05 % in PBS. Cells were examined with a LSM 510 META system, using an Axiovert 135 microscope equipped with a Plan-Neofluar 100×/1.3 objective (Zeiss, Oberkochen, Germany). YFP was investigated at $\lambda_{exc.}$ 488/$\lambda_{em.}$ 505–550 nm, AlexaFluor®647 $\lambda_{exc.}$ 633/$\lambda_{em.}$ 650–710 nm and trypan blue $\lambda_{exc.}$ 543/$\lambda_{em.}$ >590 nm. The thickness of optical sections was <0.9 µm.

Cell surface biotinylation

Cell surface biotinylation was performed as described [32]. Briefly, cells were incubated for 60 min at 4 °C with 0.4 mg/ml EZ-link-NHS-SS-biotin (Pierce, Rockford, IL, USA) in PBS with Ca^{2+}/Mg^{2+}. 50 mM glycine in PBS with Ca^{2+}/$Mg^{2+}$was used for quenching. Lysis was performed in RIPA buffer (50 mM Tris/HCl, pH 7.5; 150 mM NaCl; 1 mM EDTA; 1 % Nonidet-P40 (Calbiochem); 0.5 % Na-deoxycholate, 0.1 % Na-dodecylsulfate) with Complete Protease Inhibitor Cocktail (Roche, Indianapolis, IN, USA). The 10,000×*g* supernatant was incubated with UltraLink immobilized NeutrAvidin™ Protein Plus (Pierce, Rockford, IL, USA) for 2 h on a shaker at 4 °C. Beads were washed four times with RIPA buffer containing Complete Protease Inhibitor Cocktail (Roche, Indianapolis, IN, USA). Bound proteins were eluted with Laemmli buffer and analyzed by SDS-PAGE and Western blot with anti-GFP antibodies. For each claudin-YFP construct, the intensities of the immunoreactive bands were normalized to the respective intensity for Cld_{WT}-YFP detected in parallel. Surface biotinylation rate was calculated by dividing the normalized intensity in the cell surface fraction by the normalized intensity in the lysate.

Cellular cCPE-binding assay

Two days after transient transfection or 1 day after plating of stable lines, HEK293 cells expressing claudin constructs

were incubated with 0.5 µg/ml GST-cCPE constructs (30 min. 37 °C) in 24 well plates (Techno Plastic Products AG, Trasadingen, Switzerland). cEND cells were prepared as described above and incubated with 5 µg/ml GST-cCPE (30 min. 37 °C). Cells were washed twice with ice-cold PBS (with Ca^{2+} and Mg^{2+}), fixed (10 min with 2.4 % (w/v) paraformaldehyde in PBS) followed by quenching (20 min with 100 mM glycine in PBS) and blocking (10 min with 1 % (w/v) BSA, 0.05 % (v/v) Tween 20 in PBS). Cells were incubated with PhycoLink® anti-GST-R-phycoerythrin conjugate in 1 % (w/v) BSA; 0.05 % (v/v) Tween 20; 2 µM Hoechst 33258 in PBS for 1 h and washed 3x with PBS. Bound GST-cCPE was detected via fluorescence intensity of PhycoLink® anti-GST at $\lambda_{exc.} = 545 \pm 12$ nm/$\lambda_{em.}$ 578 ± 12 nm; claudins were detected at $\lambda_{exc.}$ 506 + 5 nm/$\lambda_{em.}$ 525 ± 5 nm for YFP tagged-, or $\lambda_{exc.}$ 488 ± 5 nm/$\lambda_{em.}$ 510 ± 5 nm for GFP-tagged claudins. Cell number was monitored with Hoechst dye at $\lambda_{exc.}$ 365 ± 12 nm/$\lambda_{em.}$ 480 ± 12 nm. Non-transfected HEK293 cells were used as a negative control (fluorescence intensity of GST-cCPE bound to $Cld3_{WT}$ was 15.4 ± 0.8 times higher than the negative control). Fluorescence intensity of bound cCPE was normalized to amount of claudins (YFP or GFP intensity) or cell number (Hoechst intensity).

Equilibrium dissociation constants (K_d) were determined in cellular cCPE-binding assays with stably Cld5-expressing HEK293 cells and varying concentrations of the GST-cCPE constructs (1–4600 nM). The cells were fixed directly after cCPE incubation, without a previous washing step. The normalized fluorescence intensity of bound cCPE was plotted against the cCPE concentration. K_d was calculated using the non-linear regression analysis for a single-site, specific binding in GraphPad Prism version 5.0 (San Diego, CA). Non-specific binding was accounted for by subtracting the fluorescence signal yielded for non-transfected HEK293 cells after GST-cCPE incubation at the respective concentrations.

Structural bioinformatics and molecular modeling

Based on the crystal structure of murine Cld15 (PDB ID: 4P79, [3]), homology models of Cld1, Cld3, Cld4 and Cld5 were created. The alignment between murine Cld15, murine Cld1, murine Cld3, human Cld4 and murine Cld5 (Fig. S1) reveals a similarity score of 55 % (Cld1), 59 % (Cld3), 61 % (Cld4) and 48 % (Cld5). Gaps and extensions in the loop regions of the structural template were adjusted manually. For interaction models of the ECL2 with cCPE, on the one hand, the cCPE crystal structure was used as deposited (PDB ID: 2QUO, [12]); on the other hand, the interaction models were built consulting our previously reported ECL2 models and cCPE interactions models [1, 9, 32]. All manual reciprocal dockings, manipulations, optimizations of ECL2 models or cCPE models ($cCPE_{Y306W}$, $cCPE_{S313H}$ and $cCPE_{Y306W/S313H}$, based on PDB ID: 2QUO), as well as calculations of hydrophobic and electrostatic potentials on the molecular surfaces, were performed with Sybyl X2.0 (Certara USA Inc., St. Louis, MO, USA). Models were energetically minimized using the AMBER7 FF99 force field.

Statistics

Unless stated otherwise, results are shown as mean ± SEM. Statistical analyses were performed using GraphPad Prism version 5.0 (San Diego, CA). Firstly, normality tests were performed (D'Agostino and Pearson omnibus, Shapiro–Wilk and Kolmogorov–Smirnov test). Data sets showing normal distribution were analyzed using an unpaired, one-tailed Student's t test. Data sets not showing normal distribution were analyzed using Wilcoxon Signed Rank Test. $p < 0.05$ was taken as significant.

Results

The sequence of the claudin ECL2 turn—comprising the residues N/D, P, L/M/V, V/T, P/A/D—is essential for CPE interaction [30]. Relative to the highly conserved proline in this turn [1, 37, 38], residue positions prior and following that proline are designated here as P−1, P, P+1, P+2, P+3; (Fig. 1a). This designation helps in the following position-dependent analysis of cCPE interaction with different claudins and their mutants.

Claudins: substitutions in Cld1 and Cld5 that mimic Cld3, enhance cCPE-binding

Cld3 and Cld4 share a common sequence motif in the turn region of ECL2 ($N^{(P-1)}$ $P^{(P)}$ $L/M^{(P+1)}$ $V^{(P+2)}$ $A/P^{(P+3)}$) which mediates cCPE-binding [9, 30]. We analyzed specific residues (P−1, P+1 and P+2; Fig. 1a) of the turn region of Cld1, Cld3 and Cld5, and their contributions to the binding of $cCPE_{WT}$. Cld1 exhibits the sequence $_{150}D^{(P-1)}$ $P^{(P)}$ $L^{(P+1)}$ $T^{(P+2)}$ $P^{(P+3)}$ and Cld5, the sequence $_{149}D^{(P-1)}$ $P^{(P)}$ $T^{(P+1)}$ $V^{(P+2)}$ $P^{(P+3)}$ (Fig. 1a). $Cld1_{WT}$ shows only weak binding of $cCPE_{WT}$ while $Cld5_{WT}$ does not bind $cCPE_{WT}$ when compared to $Cld3_{WT}$ (Fig. 1b, c). Cld3-mimicking constructs of Cld1, $Cld1^{(P-1)}_{D150N}$ and $Cld1^{(P+2)}_{T153V}$, showed increased binding of $cCPE_{WT}$. Interestingly, $Cld1^{(P+2)}_{T153V}$ displayed a much greater increase in cCPE-binding than did $Cld1^{(P-1)}_{D150N}$. Surprisingly, double substitution of positions P−1 and P+2 ($Cld1^{(P-1)/(P+2)}_{D150N/T153V}$) gave the lowest increase in binding (Fig. 1b). We next analyzed the effect of Cld3-mimicking substitutions of Cld5 at positions

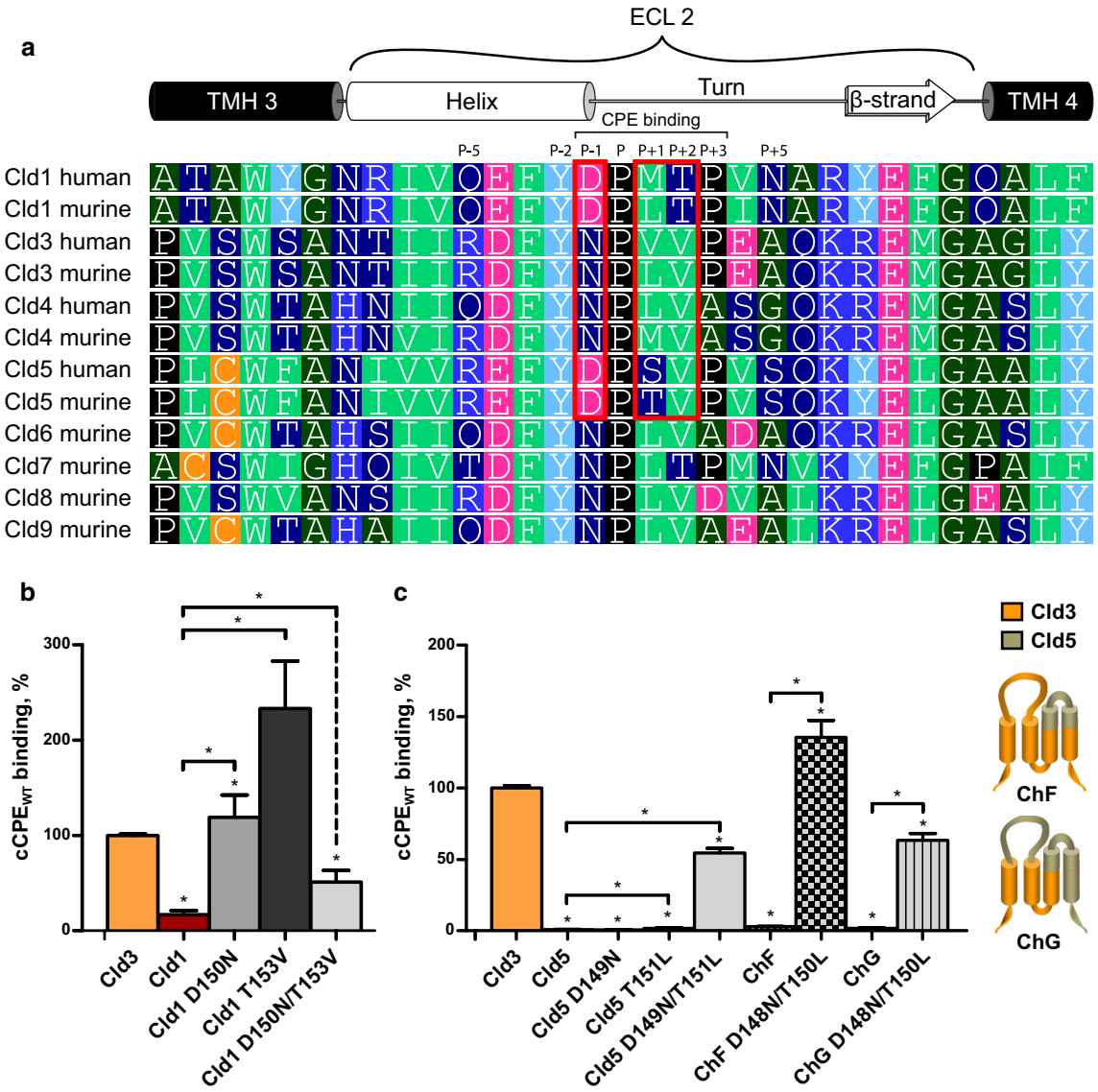

Fig. 1 Residues at Positions P−1, P+1 and P+2 inhibit binding of cCPE to Cld1 and Cld5. **a** Sequence alignment of ECL2 (extracellular loop 2) of Cld1, −3, −4 to −9 (ClustalW2) displayed using Geneious Pro 5.4.4. *Red frame:* striking difference between Cld3 and Cld4 and Cld1 and Cld5. *green:* bulky hydrophobic; *dark green:* small hydrophobic; *dark blue:* polar uncharged; *blue:* basic; *magenta:* acidic; *cyan:* Tyr; *black:* Pro; *orange:* Cys. Helix, Turn and β-strand: secondary structure elements of the ECL2; CPE-binding: core residues of the CPE-binding region; TMH: transmembrane helix. **b** HEK293 cells transiently expressing Cld3$_{WT}$ (orange columns), Cld1$_{WT}$ (*red columns*) or Cld3-mimicking Cld1 mutants (*gray columns*) and **c** HEK293 cells transiently expressing Cld3$_{WT}$ (*orange columns*), Cld5$_{WT}$ (*beige columns*), Cld3-mimicking Cld5 mutants (*gray columns*) or Cld3/Cld5 chimeras (ChF, ChG, checkered and striped columns, scheme on the right depicts Cld3 (*orange*) and Cld5 (*beige*) portions of the chimeras) were incubated with 0.5 µg/ml GST-cCPE$_{WT}$. Bound cCPE was detected using anti-GST antibodies in a plate reader. **b** cCPE$_{WT}$ binds to the Cld3-mimicking Cld1 mutants (Cld1$_{D150N}$; Cld1$_{T153V}$; Cld1$_{D150N/T153V}$) more strongly than to Cld1$_{WT}$. **c** cCPE$_{WT}$ binds to the Cld3-mimicking Cld5 mutant Cld5$_{D149N/T151L}$ and the Cld3/Cld5 chimeric mutants (ChF$_{D148N/T150L}$ and ChG$_{D148N/T150L}$) much more strongly than to Cld5$_{WT}$ or to ChF and ChG. Results are mean ± SEM ($n \geq 5$); *$p < 0.05$

P−1 (Cld5$^{(P-1)}_{D149N}$) and P+1 (Cld5$^{(P+1)}_{T151L}$) and their double mutant (Cld5$^{(P-1)/(P+1)}_{D149N/T151L}$). In contrast to Cld1, the single mutants Cld5$^{(P-1)}_{D149N}$ and Cld5$^{(P+1)}_{T151L}$ revealed no or only very slightly increased binding of cCPE$_{WT}$. Only the double mutant Cld5$^{(P-1/P+1)}_{D149N/T151L}$ showed greatly increased binding of cCPE$_{WT}$ (Fig. 1c). Similarly, the corresponding double substitution D148N/T150L in Cld3/Cld5 chimeras containing the ECL2 (ChF) and ECL1 (ChG) of Cld5 and the rest of Cld3 strongly increased the binding of cCPE$_{WT}$ (Fig. 1c).

This indicates that these residues (P−1 and P+1 in Cld5 or P+2 in Cld1) of the ECL2 turn region interfere with

cCPE-binding to Cld1 and Cld5. Nevertheless, the changes in cCPE-binding to HEK293 cells expressing the Cld3-mimicking constructs could also be due to differences in the availability of the mutants for cCPE on the cell surface. Therefore, the subcellular localization of Cld3-mimicking mutants of Cld1 and Cld5 was analyzed by confocal microscopy, in comparison to the respective Cld_{WT}. We detected $Cld1_{WT}$ and $Cld5_{WT}$ enrichment at contacts between two claudin-expressing cells (Fig. S2A, B), as demonstrated previously [33]. This indicates *trans*-interaction between claudins. A similar enrichment was obtained for $Cld1^{(P-1)}_{D150N}$, $Cld1^{(P+2)}_{T153V}$, $Cld1^{(P-1)/(P+2)}_{D150N/T153V}$, $Cld5^{(P-1)}_{D149N}$ and $Cld5^{(P+1)}_{T151L}$. $Cld5^{(P-1)/(P+1)}_{D149N/T151L}$ exclusively displayed marked loss of contact enrichment, indicating that only for $Cld5^{(P-1)/(P+1)}_{D149N/T151L}$ *trans*-interaction was directly or indirectly affected (Fig. S2A, B). To analyze whether the mutations affect the amount of claudins in the plasma membrane, cell surface biotinylation was performed (Fig. S2C). Only the mutations $T151L^{(P+1)}$ and D149 N/$T151L^{(P-1)/(P+1)}$ in Cld5 clearly reduced the levels of claudin in the plasma membrane; Nevertheless, confocal microscopy analyses showed that Alexa647-cCPE binds to HEK293 cells expressing $Cld5_{D149N/T151L}$-YFP (Fig. S2B, panel III). In addition, neither microscopy nor surface biotinylation indicated increased levels of $Cld1^{(P-1)}_{D150N}$, $Cld1^{(P+2)}_{T153V}$ or $Cld1^{(P-1)/(P+2)}_{D150N/T153V}$ in the plasma membrane. Furthermore, the Cld3/Cld5 chimeras ChF and ChG occurred at high levels in the plasma membrane and their subcellular distribution was essentially unchanged by D148N/T150L substitution (ChF, [34] and ChG, unpublished data). In summary, the results exclude the possibility that the differences in cCPE-binding to these constructs are due to differences in their subcellular localization. All analyzed claudin constructs reached the plasma membrane. This indicates that the substitutions did not induce misfolding of the protein which would interfere with the binding assays.

Taken together, our data indicate that residues of the ECL2 turn region at positions P−1, P+1 in Cld5 and at positions P−1, P+2 in Cld1 prevent strong interaction with cCPE. Consequently, to create cCPE-constructs with extended binding to $Cld5_{WT}$, cCPE has to be modified in such a way that it is able to complement the differences in the turn region of the ECL2 of Cld1 and Cld5 relative to Cld3 and Cld4.

cCPE: *in silico* analysis of interaction with Cld1 and Cld5 identified cCPE positions that can be modified to enhance binding

Utilizing previously established interaction models of cCPE with the ECL2 of Cld3 and Cld4 [9], we generated working models for the interaction of cCPE with Cld1 and Cld5 (Fig. 2). The interaction models indicated how the ECL2 turn fits into the hydrophobic binding pocket of cCPE. The previous homologous interaction model of cCPE and Cld3 indicates that ECL2 turn positions P−1 (Asn^{149} in Cld3, Asp^{150} in Cld1 and Asp^{149} in Cld5) and P+2 (Val^{152} in Cld3, Thr^{153} in Cld1 and Val^{152} in Cld5) lie on the peripheral rim of the binding pocket, which consists of two pits. The large hydrophobic pit (triple-Tyr pit) of cCPE is formed by a triple-Tyr motif (Tyr^{306}, Tyr^{310} and Tyr^{312}). Cld3 and Cld4 contain a large and bulky hydrophobic side chain at P+1 (Leu^{150} and Leu^{151}, respectively), completely filling the space of the triple-Tyr pit (Fig. 2b). Unlike all reported cCPE-binding claudins (e.g., Cld3 and Cld4), Cld5 lacks this bulky hydrophobic residue at P+1 of the ECL2—which was previously determined to be a key interaction partner for cCPE [9]. The smaller residues, $Thr^{(P+1)}$ of murine or $Ser^{(P+1)}$ of human Cld5, are unable to fill the triple-Tyr pit of cCPE (Fig. 2d). These findings lead to the conclusion that the triple-Tyr pit of cCPE requires modification (downsizing) to fit to Thr/$Ser^{151(P+1)}$ of Cld5. Downsizing the triple-Tyr pit (magenta arrows in Fig. 2d) should compensate for the void space, as left by the lack of a large hydrophobic residue at position P+1 in Cld5 (green square in Fig. 2d). This should enable binding of cCPE to Cld5 and lead to a cCPE-variant with shifted specificity towards Cld5. In this study, we will refer to this cCPE-modification as "pit-filler". Based on the working models, we selected the following residues Leu^{238}, Ile^{258}, Val^{259}, Ala^{302} and Tyr^{306} of cCPE as potential "pit-filler" positions.

Moreover, to enhance cCPE-binding to Cld1 or Cld5, a positively charged residue should be introduced at the peripheral rim of the triple-Tyr pit, as this can counteract the negatively charged $Asp^{(P-1)}$ of Cld1 and Cld5 (Asp^{150} and Asp^{149}, respectively, Fig. 2c, d), or interact with $Gln^{146(P-5)}$ of Cld1 ("electrostatic angler"). In the latter case, the introduction of a positive-charged residue should only enhance binding to Cld1, since Cld5 exhibits an arginine at the respective position ($Arg^{145(P-5)}$, Fig. 1a). Ser^{307} and Tyr^{310} are located at the peripheral rim of the triple-Tyr pit and thus the interaction model suggested that these positions in cCPE could be used to introduce positive or polar residues ("electrostatic angler"), to permit hydrophilic interactions with either $Asp^{(P-1)}$ in Cld1 and Cld5 or with $Gln^{(P-5)}$ in Cld1. Interestingly, substitution S307R was incorporated in multiple mutants that also apparently affect cCPE-binding to claudins [29].

cCPE: S313H of the triple serine mutant (305,307,313) contributes most to the binding of both Cld1 and Cld5

$cCPE_{S304A/S305P/S307R/N309H/S313H}$ was shown to enhance cCPE-binding to Cld1 and Cld5 and $cCPE_{S305P/S307R/S313H}$

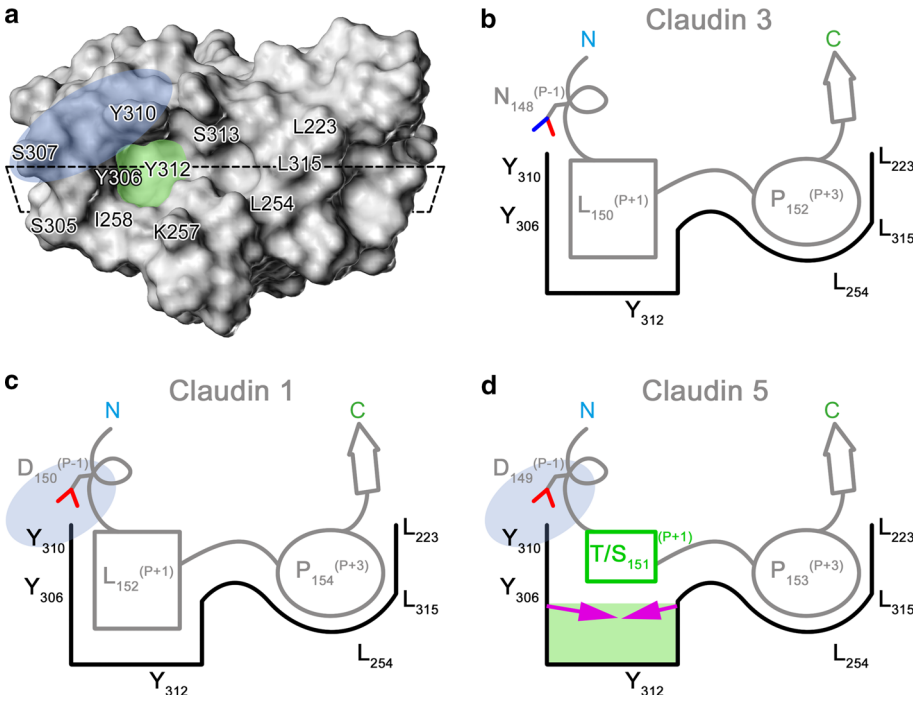

Fig. 2 Scheme of the claudin–cCPE Interaction. **a** Top view onto the surface of cCPE, (*white*) with the claudin-binding pocket and the triple-Tyr pit (*green*) and the rim of the triple-Tyr pit (*blue*). *Dashed lines* represent the cross section for the schemes. **b** Interaction of the ECL2 of Cld3 (*gray*) with the claudin-binding pocket of cCPE (black) in comparison with **c** Cld1 and **d** Cld5. Introduction of a positive-charged residue on the rim of the triple-Tyr pit which could interact with $D^{(P-1)}$ (*blue cloud*) could lead to enhanced binding of cCPE to Cld1 and Cld5. To enable binding to Cld5, the huge gap between Thr/$Ser^{(P+1)}$ (T/S) and the triple-Tyr pit (*green square*) has to be filled by substitutions around the triple-Tyr pit (*magenta arrows*, "pit-filler")

was shown to enhance cCPE-binding to Cld1 [29]. To characterize the influence of each substitution of $cCPE_{S305P/S307R/S313H}$ in detail, the corresponding cCPE single ($cCPE_{S305P}$ and $cCPE_{S313H}$), double ($cCPE_{S305P/S307R}$) and triple mutants ($cCPE_{S305P/S307R/S313H}$) were generated and their binding to Cld1- and Cld5-constructs was investigated in cellular binding assays with HEK293 cells expressing $Cld1_{WT}$, $Cld1^{(P-1)}_{D150N}$, $Cld1^{(P+2)}_{T153V}$ and $Cld1^{(P-1)/(P+2)}_{D150N/T153V}$ (Fig. 3a), or $Cld5_{WT}$, $Cld5^{(P-1)}_{D149N}$, $Cld5^{(P+1)}_{T151L}$and $Cld5^{(P-1)/(P+1)}_{D149N/T151L}$ (Fig. 3b).

Claudin-1: Compared to $cCPE_{WT}$, the mutants $cCPE_{S305P/S307R/S313H}$ and $cCPE_{S313H}$ bound more strongly to $Cld1_{WT}$ and $Cld1^{(P-1)/(P+2)}_{D150N/T153V}$, but no more strongly to $Cld1^{(P-1)}_{D150N}$ and $Cld1^{(P+2)}_{T153V}$. In contrast, $cCPE_{S307R}$ and $cCPE_{S305P/S307R}$ exhibited stronger binding only to $Cld1_{WT}$, but not to the other Cld1 constructs (Fig. 3a).

Claudin-5: Compared to $cCPE_{WT}$, $cCPE_{S305P/S307R/S313H}$ and $cCPE_{S313H}$ showed much stronger binding to $Cld5^{(P+1)}_{T151L}$, somewhat stronger binding to $Cld5_{WT}$ and $Cld5^{(P-1)}_{D149N}$ and slightly but significantly stronger binding to $Cld5^{(P-1)/(P+1)}_{D149N/T151L}$. $cCPE_{S305P/S307R}$, $cCPE_{S305P}$ and $cCPE_{S307R}$ showed no clear increase in binding to any Cld5 construct (Fig. 3b).

In summary, S307R slightly strengthens binding to Cld1 but not to Cld5. S313H increases binding to Cld1 and Cld5, and has a stronger effect on binding than does S307R. Apart from $cCPE_{S307R}$, the introduction of a positive-charged or polar residue to the rim of the triple-Tyr pit ("electrostatic angler") did not enhance binding of cCPE to Cld1 or Cld5 ($cCPE_{S307R}$, $cCPE_{Y310H}$ and $cCPE_{Y310K}$). Binding data and our model (Fig. S3) suggest that the introduced Arg^{307} of $cCPE_{S307R}$ most probably interacts with $Gln^{146(P-5)}$ of Cld1. Cld5 exhibits an $Arg^{(P-5)}$ at the corresponding position, which could explain why $cCPE_{S307R}$ shows no increased binding to Cld5 but to $Cld5_{R145Q}$, especially when combined with substitutions S305P and S313H ($cCPE_{S305P/S307R/S313H}$, Fig. S3C).

cCPE: combination of Y306W with S313H enhances specificity to Cld5

After analyzing the contributions of single substitutions S305P, S307R and S313H to the binding behavior of the broadly specific claudin binder $cCPE_{S305P/S307R/S313H}$, we studied the binding ability of the potential "pit-filler" mutants to Cld1 and Cld5. None of the single mutants ($cCPE_{L238F}$, $cCPE_{V259Y}$, $cCPE_{A302M}$, $cCPE_{A302Y}$, $cCPE_{Y306W}$) exhibited increased binding to Cld1 or Cld5 compared to $cCPE_{WT}$ in cellular binding assays (Fig. 4a). Since $cCPE_{S313H}$ showed enhanced binding to $Cld5_{WT}$, without decreasing the binding to Cld3 or Cld4, we decided to create constructs combining S313H with the potential "pit-filler" mutants. Thus, the following constructs were designed: $cCPE_{L238F/S313H}$, $cCPE_{V259Y/S313H}$, $cCPE_{A302Y/S313H}$ and $cCPE_{Y306W/S313H}$. Binding of these constructs was then compared in cellular binding assays to the binding

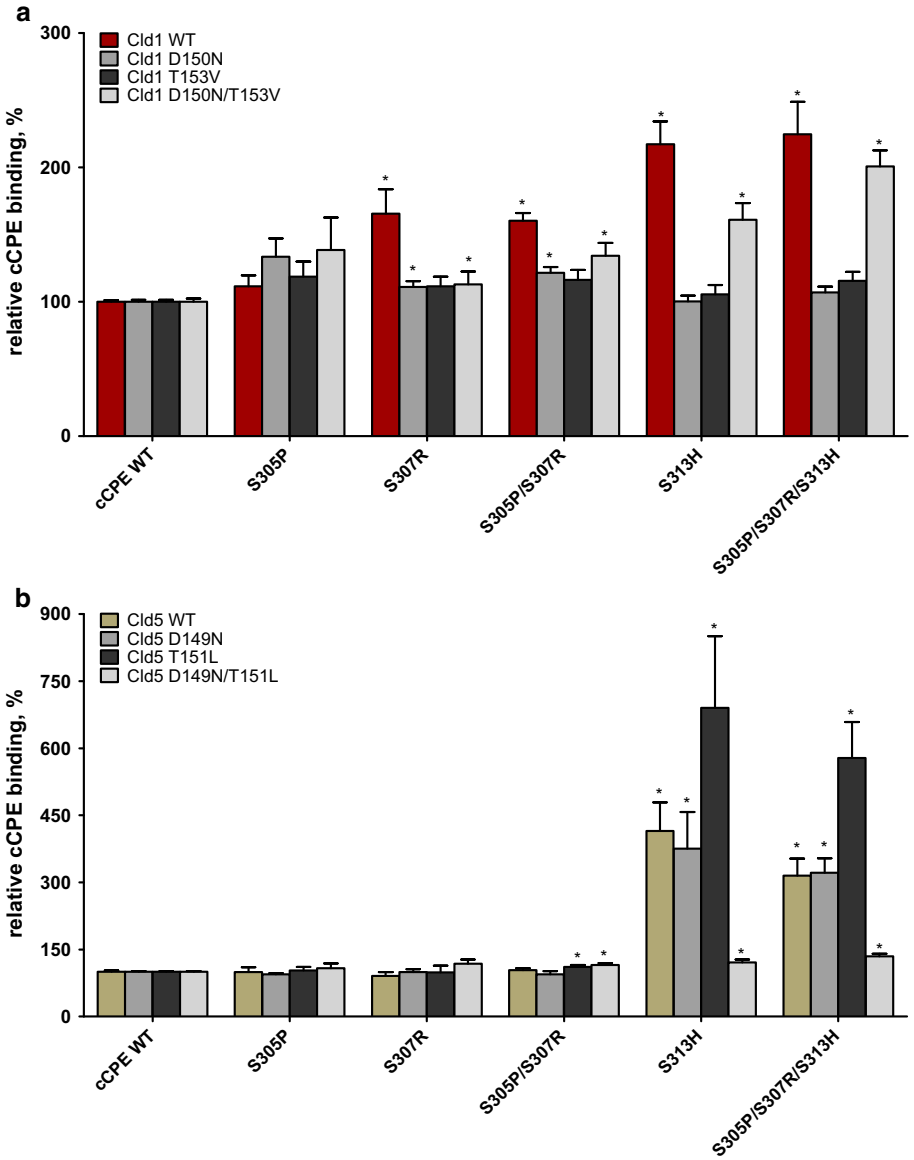

Fig. 3 Substitution S313H in cCPE makes the biggest contribution of $cCPE_{S305P/S307R/S313H}$ to binding to Cld1 and Cld5. HEK293 cells transiently expressing **a** $Cld1_{WT}$ (*red columns*), or Cld3-mimicking mutations of Cld1 (*gray columns*) or **b** $Cld5_{WT}$ (*beige columns*), or Cld3-mimicking mutations of Cld5 (*gray columns*) were incubated with 0.5 µg/ml GST-$cCPE_{WT}$ or GST-cCPE mutants. Bound cCPE was detected using anti-GST antibodies in a plate reader. Quantification normalized to $cCPE_{WT}$ (relative binding) for each claudin construct. $cCPE_{S313H}$ and $cCPE_{S305P/S307R/S313H}$ showed a strong increase in binding to $Cld1_{WT}$ and $Cld1_{D150N/T153V}$. **a** $cCPE_{S307R}$ only showed a strong increase in binding to $Cld1_{WT}$. **b** Only $cCPE_{S313H}$ and $cCPE_{S305P/S307R/S313H}$ showed a strong increase in binding to $Cld5_{WT}$, $Cld5_{D149N}$ and $Cld5_{T151L}$, but not to $Cld5_{D149N/T151L}$. Results are mean ± SEM ($n \geq 5$); $^*p < 0.05$

of $cCPE_{WT}$ and $cCPE_{S313H}$ to $Cld1_{WT}$ and $Cld5_{WT}$ (Fig. 4b).

Relatively to $cCPE_{WT}$, $cCPE_{V259Y/S313H}$ demonstrated decreased binding to Cld1 and Cld5. $cCPE_{L238F/S313H}$ and $cCPE_{A302Y/S313H}$ showed stronger binding to Cld1 and Cld5 but bound more weakly than $cCPE_{S313H}$. In contrast, $cCPE_{Y306W/S313H}$ bound much more strongly to Cld5 with a significant increase compared to $cCPE_{S313H}$. $cCPE_{Y306W/S313H}$ exhibited decreased binding to $Cld1_{WT}$ compared to $cCPE_{S313H}$.

To analyze the mechanism by which $cCPE_{Y306W/S313H}$ enhanced cCPE-binding to Cld5 in more detail, we conducted cellular binding assays with HEK293 cells expressing $Cld5_{WT}$, and the Cld3-mimicking mutants $Cld5^{(P-1)}_{D149N}$, $Cld5^{(P+1)}_{T151L}$ or $Cld5^{(P-1)/(P+1)}_{D149N/T151L}$ (Fig. 5a). In contrast to the binding of $cCPE_{WT}$ to the respective Cld5 construct, $cCPE_{Y306W/S313H}$ showed marked increases in binding to both $Cld5_{WT}$ and $Cld5^{(P-1)}_{D149N}$; in both cases, the binding was stronger than with $cCPE_{S313H}$. In addition, $cCPE_{S313H}$ showed the greatest increase in binding to $Cld5^{(P+1)}_{T151L}$ and also slightly enhanced binding to $Cld5^{(P-1)/(P+1)}_{D149N/T151L}$. As predicted for a "pit-filler" mutant, our designed construct $cCPE_{Y306W/S313H}$ showed weaker binding than $cCPE_{S313H}$ to $Cld5^{(P+1)}_{T151L}$ and to $Cld5^{(P-1)/(P+1)}_{D149N/T151L}$. In addition, we analyzed the binding of these cCPE-constructs ($cCPE_{Y306W/S313H}$, $cCPE_{S313H}$, $cCPE_{WT}$ and, as negative control, $cCPE_{Y306A/L315A}$) to Cld1, −3, −4, −5, −6, −7, −8 and −9 (Fig. 5b). Compared to $cCPE_{WT}$, the combined double mutant $cCPE_{Y306W/S313H}$

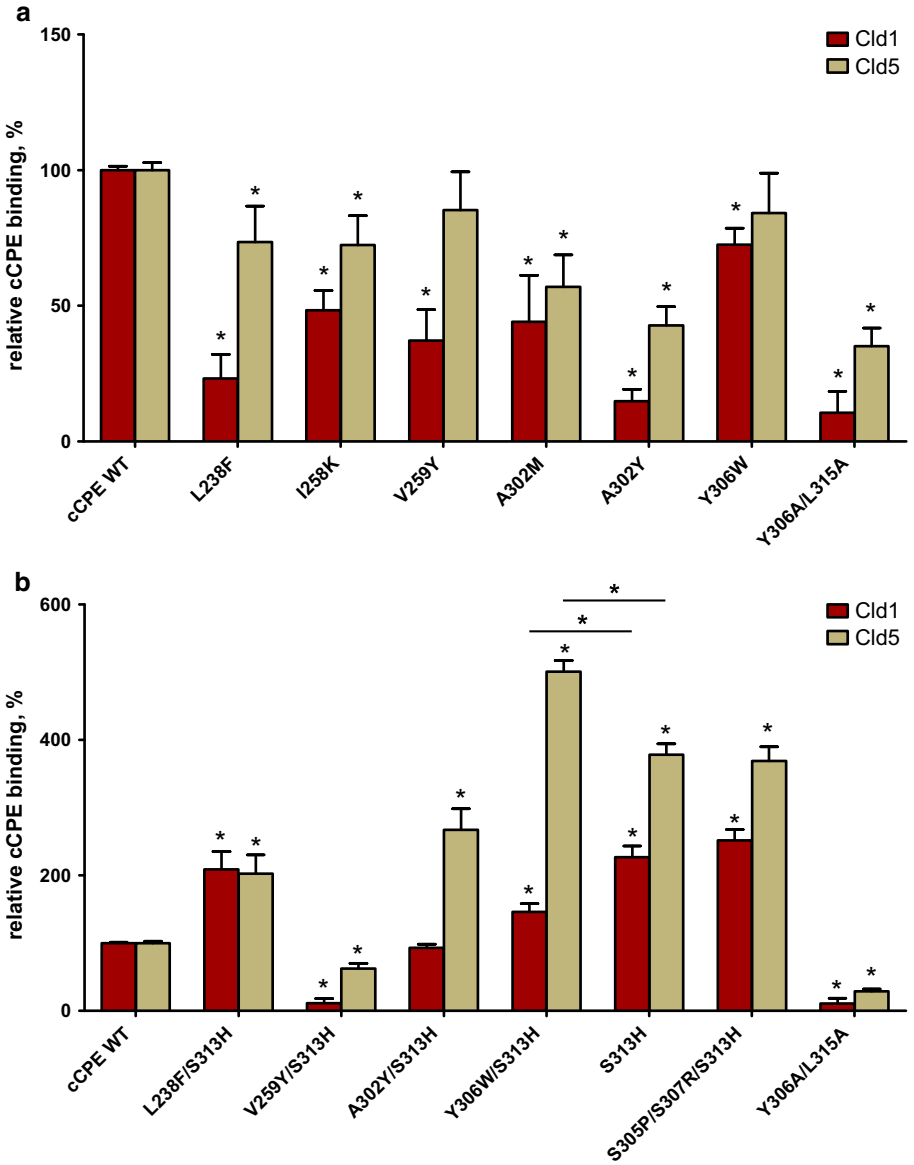

Fig. 4 $cCPE_{Y306W/S313H}$ shows increased binding to Cld5. HEK293 cells transiently expressing $Cld1_{WT}$ (*red columns*), $Cld5_{WT}$ (*beige columns*) were incubated with 0.5 µg/ml GST-$cCPE_{WT}$, **a** GST-cCPE single mutants, **b** GST-cCPE double mutants containing substitution S313H and GST-$cCPE_{Y306A/Y315A}$ as negative control. Bound cCPE was detected using anti-GST antibodies in a plate reader. Quantification normalized to $cCPE_{WT}$ (relative binding) for the respective Cld_{WT}. **a** Only $cCPE_{V259Y}$ and $cCPE_{Y306W}$ show binding to Cld1 or Cld5 which closely resembles that of $cCPE_{WT}$. **b** $cCPE_{Y306W/S313H}$ shows increased binding to Cld5 compared to $cCPE_{S313H}$ and $cCPE_{WT}$ while also showing weaker binding to Cld1 compared to $cCPE_{S313H}$. Results are mean ± SEM ($n \geq 5$); $^*p < 0.05$

showed weaker binding to Cld3, −4, −6, −7, −8 and −9, the strongest binding to Cld5 and slightly stronger binding to Cld1.

cCPE: Y306W/S313H binds to Cld5 with a nanomolar K_d

To quantify the affinity of $cCPE_{Y306W/S313H}$ for $Cld5_{WT}$, concentration-dependent binding of the cCPE-variant to Cld5-expressing HEK293 cells was analyzed. $cCPE_{Y306W/S313H}$ bound to $Cld5_{WT}$ with a K_d of 33 ± 10 nM ($n = 5$). In contrast, the K_d value for $cCPE_{WT}$ could not be determined precisely, since even with high $cCPE_{WT}$ concentrations (up to 4600 nM), the binding was not clearly saturated (Fig. 5c). However, this result indicates that the K_d of $cCPE_{WT}$ for $Cld5_{WT}$ is at least $\gg$1.0 µM and therefore the affinity of cCPE to $Cld5_{WT}$ was increased at least 30-fold by the Y306W/S313H substitution.

cCPE: Y306W/S313H shows enhanced binding to cells with endogenous Cld5

To investigate whether the positive effect of $cCPE_{Y306W/S313H}$ on binding to Cld5 can also be observed in cells expressing Cld5 endogenously, we used the brain microvascular endothelial cEND cell line. These cells have been shown to express Cld5 at the protein and mRNA levels and are used as an in vitro model for the blood–brain barrier

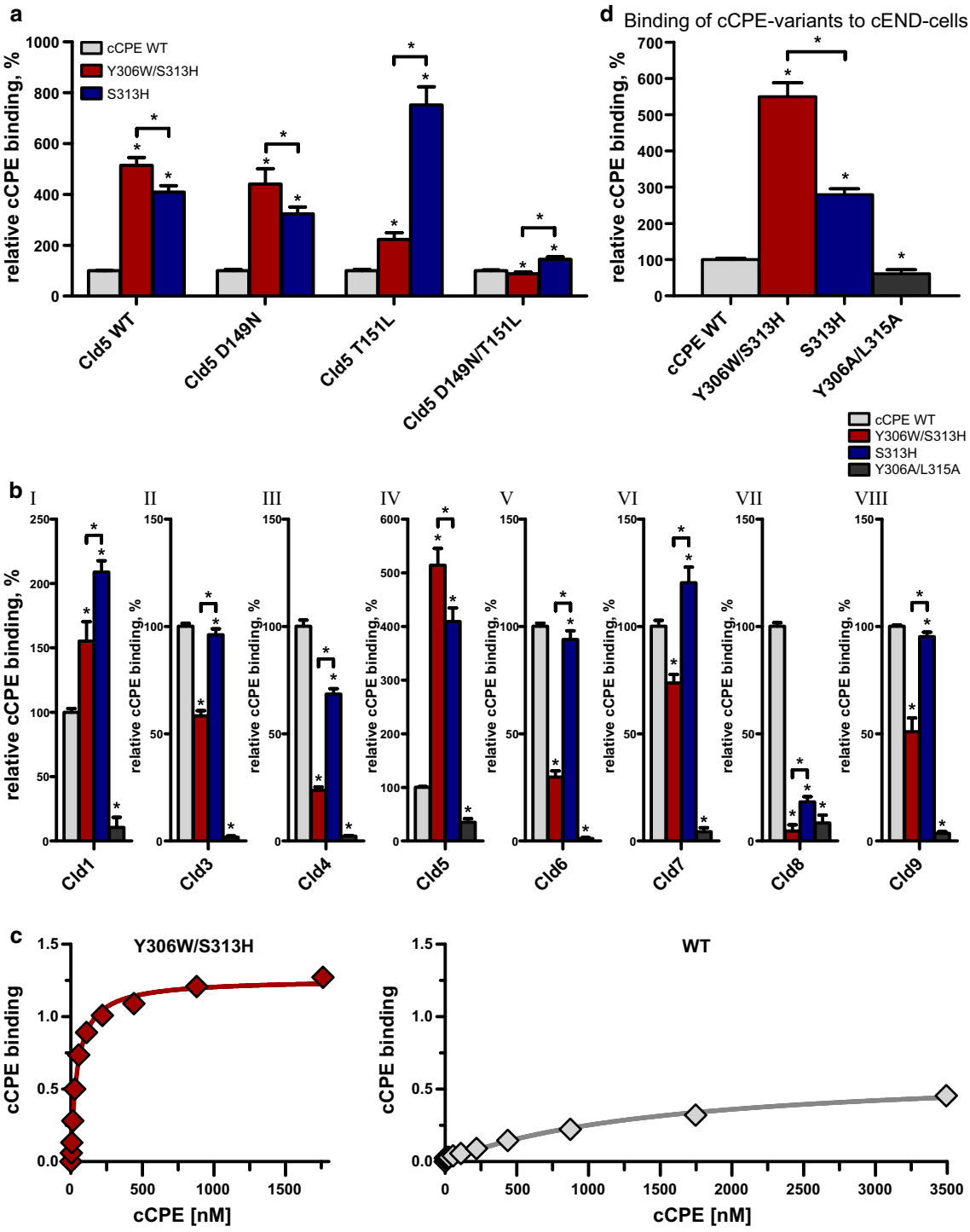

[39, 40]. We performed cellular binding assays of $cCPE_{WT}$, $cCPE_{S313H}$, $cCPE_{Y306W/S313H}$ and $cCPE_{Y306A/L315A}$ with this cell line (Fig. 5d). $cCPE_{Y306W/S313H}$ showed a fivefold increased binding to cEND cells compared to the binding of $cCPE_{WT}$ and a 2.5-fold increased binding compared to $cCPE_{S313H}$. This validates the enhanced binding of $cCPE_{Y306W/S313H}$ to Cld5 observed in HEK293 cells in a cellular system expressing Cld5 endogenously.

◀**Fig. 5** $cCPE_{Y306W/S313H}$ shows shifted specificity towards Cld5 and enhanced binding to cEND cells. HEK293 cells **a** transiently expressing $Cld5_{WT}$, or Cld3-mimicking mutations of Cld5 or **b** transiently expressing (I) $Cld1_{WT}$, (IV) $Cld5_{WT}$ or stably expressing (II) $Cld3_{WT}$, (III) $Cld4_{WT}$ and (V) Cld6 $_{WT}$—(VIII) $Cld9_{WT}$ were incubated with 0.5 µg/ml GST-$cCPE_{WT}$ (*gray columns*), GST-$cCPE_{Y306W/S313H}$ (*red columns*), GST-$cCPE_{S313H}$ (*blue columns*) or GST-$cCPE_{Y306A/L315A}$ (*black columns*) as negative control. Bound cCPE was detected using anti-GST antibodies in a plate reader. **a** $cCPE_{Y306W/S313H}$ binds better to $Cld5_{WT}$ and $Cld5_{D149N}$ than $cCPE_{S313H}$ and $cCPE_{WT}$, but binds more weakly to $Cld5_{T151L}$ and $Cld5_{D149N/T151L}$ than $cCPE_{S313H}$. **b** $cCPE_{Y306W/S313H}$ binds better to $Cld5_{WT}$ than $cCPE_{S313H}$ and $cCPE_{WT}$ and better to $Cld1_{WT}$ than $cCPE_{WT}$ but not better than $cCPE_{S313H}$. $cCPE_{Y306W/S313H}$ binds more weakly than does $cCPE_{WT}$ to all other claudins. Results are mean ± SEM ($n \geq 5$); $^*p < 0.05$. **c** Representative concentration-dependent binding of GST-$cCPE_{WT}$ (*gray line*) and GST-$cCPE_{Y306W/S313H}$ (*red line*) to stably Cld5-expressing HEK293 cells used for determination of K_d. **d** cEND cells, which endogenously express Cld5, were incubated with 5 µg/ml cCPE-Variants. Bound cCPE was detected using anti-GST antibodies in a plate reader. Quantification normalized to $cCPE_{WT}$ (relative binding). Results are mean ± SEM ($n \geq 5$); $^*p < 0.05$

Interestingly, the difference in binding between $cCPE_{Y306W/S313H}$ and $cCPE_{S313H}$ even exceeds the difference observed in the HEK293 cell system.

Discussion

We aimed to understand the mechanism by which *Clostrisium perfringens* enterotoxin binds selectively and with high affinity to distinct claudins. In this study, we used a structure-based rational molecular approach to reveal mechanistic details about the cCPE–claudin interactions and indirectly to deduce information about the extracellular structural properties of interacting claudins, particularly Cld1 and Cld5. Insights into the interaction were gained by combining structural information, molecular modeling, cellular binding assays and mutagenesis. Firstly, we asked the question as to why cCPE only interacts weakly or not at all with Cld1 and Cld5. By sequence comparison, we identified two key differences between Cld1 and Cld5 and other claudins interacting with cCPE, namely $Asp^{150(P-1)}$ and $Thr^{153(P+2)}$ in Cld1 and $Asp^{149(P-1)}$ and $Thr^{151(P+1)}$ in Cld5 (Fig. 1a). Subsequently we created Cld3-mimicking mutants of Cld1 and Cld5 and analyzed their cCPE-binding behavior. Furthermore, we can provide a molecular explanation as to why the core substitutions of the cCPE-variants ($cCPE_{S305P/S307R/S313H}$) reported by Takahashi et al. [29] enhance Cld1 binding and allow Cld5 binding.

Our main goal, however, was to combine the knowledge gained from these analyses to create a cCPE-variant with a high affinity and a shifted specificity towards Cld5, which is not naturally bound by $cCPE_{WT}$. This could be used for the development of a blood–brain barrier modulator.

Claudins: ECL2 conformations differ as a result of $Asp^{(P-1)}$ (Cld1 and Cld5) or $Asn^{(P-1)}$ (Cld3 and Cld4)

The conformation of the ECL2 differs depending on the amino acid residue at position P−1. The results of the cellular binding assays of the Cld3-mimicking mutants of Cld1, Cld5 and the Cld3/Cld5 chimeras show that presence of $Asp^{(P-1)}$ drastically disturbs the interaction of cCPE with Cld1 and Cld5 (Fig. 1b, c); this is in line with the results of the substitution of $Asn^{(P-1)}$ to Asp in Cld3 and Cld4 [8, 9] and the substitution mapping of ECL2 peptides of Cld3 and Cld5 [30]. Firstly, it was assumed that $Asp^{(P-1)}$ in claudins interrupts the binding of cCPE due to electrostatic interference with residues on the peripheral rim of the binding pocket. However, our results for $cCPE_{S307R}$, $cCPE_{S305P/S307R}$ and $cCPE_{S305P/S307R/S313H}$ provided no evidence for a direct interaction of $Asp^{(P-1)}$ in Cld1 and Cld5 with Arg^{307} or His^{313} in cCPE (Fig. 3). According to our data, position Arg^{307} in cCPE seems rather to interact with $Gln^{(P-5)}$ of Cld1 (Fig. S3), which further confirms not only our previously reported cCPE–ECL2 interaction models of Cld3 and Cld4 [9], but also is in agreement with our current interaction model between cCPE and ECL2 of Cld5 (Figs. 2, 6), where the N-terminal helix of the ECL2 of Cld1 and Cld5 lies across the triple-Tyr pit.

All of these results indicate that the different cCPE-binding behavior of $Asp^{(P-1)}$ and $Asn^{(P-1)}$ in ECL2 of claudins is more probably caused by an altered intramolecular conformation of the turn region of the ECL2 of Cld1 and Cld5 compared to the ECL2 of Cld3 and Cld4. According to the ECL2 models, $Asp^{(P-1)}$ of Cld1 and Cld5 is able to form a stronger H-bond network with the backbone amide hydrogens of the residues P+1 and P+2 and/or one hydroxyl group ($Thr/Ser^{(P+1)}$ Cld5 and $Thr^{(P+2)}$ Cld1) compared to just one possible interaction for $Asn^{(P-1)}$ of Cld3 and Cld4 (Fig. 6). This leads to a more intra-turn orientation of the side chain of residue P+2—$Thr^{153(P+2)}$ (Cld1) and $Val^{152(P+2)}$ (Cld5), making the ECL2 of Cld1 and Cld5 slimmer and more rigid compared to the protruding conformation of residue P+2 in the bulkier ECL2 of Cld3 or Cld4 (Fig. 6). This slimmer conformation of the ECL2 would explain the positive effect of the substitution S313H in $cCPE_{S313H}$, $cCPE_{S305P/S307R/S313H}$ and $cCPE_{Y306W/S313H}$ on binding to Cld1 and Cld5.

$Cld5^{(P-1)}_{D149N}$ does not bind cCPE due to the lack of a bulky hydrophobic residue (Leu) at position P+1 that fills the triple-Tyr pit of cCPE. However, the Cld5 mutant containing Leu at position P+1, $Cld5^{(P+1)}_{T151L}$ does not bind cCPE well, since it still possesses the slimmer and more rigid turn conformation of $Cld5_{WT}$ caused by $Asp^{149(P-1)}$. This is supported by the finding that $cCPE_{S313H}$, which fits better

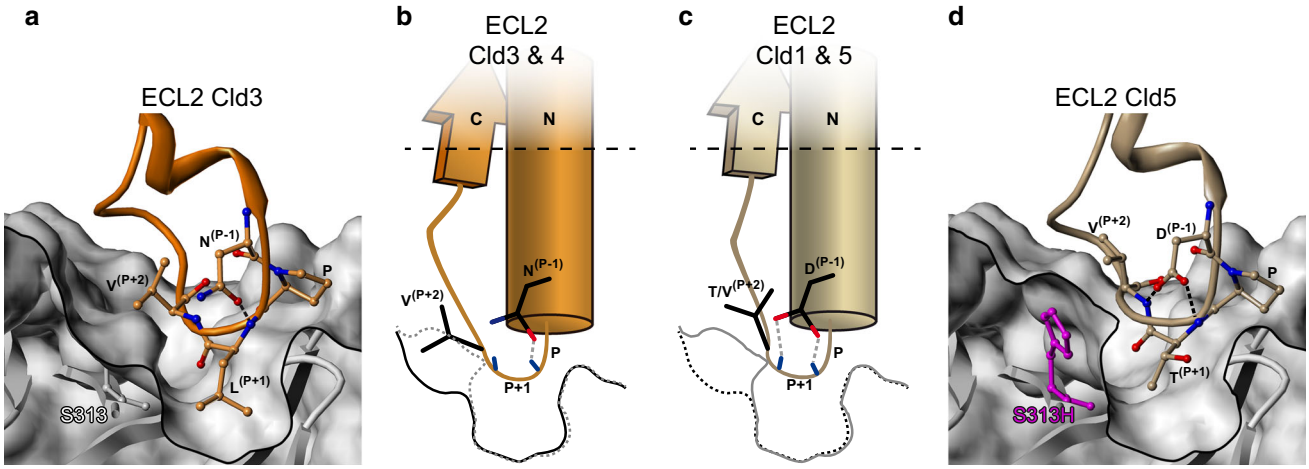

Fig. 6 Suggested conformational differences in the turn region of ECL2 of Cld1 and Cld5 compared to Cld3 and Cld4. cCPE is illustrated (*cartoon*, *white*) with the calculated surface (*white*); substituted residues are depicted as ball and stick in *magenta*. **a** Cross section of the detailed interaction model of $cCPE_{WT}$ with the Cld3-ECL2 (*cartoon*, *orange*, with the turn defining residues as ball and stick; *red*: oxygen, *blue*: nitrogen). **b** Sketch of the interaction of the ECL2 of Cld3 and Cld4 (*orange*, *dashed line*: possible H-bond with backbone amid; *red*: oxygen, *blue*: nitrogen) and the claudin-binding pocket of $cCPE_{WT}$ (black line) and $cCPE_{S313H}$ (dashed gray line). **c** Sketch of the interaction of the ECL2 of Cld1 and Cld5 (*beige*, *dashed lines*: possible H-bonds with backbone amides; *red*: oxygen, *blue*: nitrogen) and the claudin-binding pocket of $cCPE_{WT}$ (*dashed black line*) and $cCPE_{S313H}$ (*gray line*). **d** Cross section of the detailed interaction model of $cCPE_{S313H}$ with the Cld5-ECL2 (*cartoon*, *beige*, with the turn defining residues as ball and stick; *red*: oxygen, *blue*: nitrogen). The residue at position P-1 has a crucial influence on the structure of the ECL2. **a**, **b** While $Asn^{(P-1)}$ (Cld3 and Cld4) can only form one hydrogen bond with the backbone amides of the ECL2-turn region and thus causes a more flexible and wider ECL2-structure which fits optimally for $cCPE_{WT}$, **c**, **d** $Asp^{(P-1)}$ of Cld1 and Cld5 can form a hydrogen bond network with two backbone amides of the ECL2-turn region and the polar side chain of $Thr^{(P+1)}$ (Cld5) or $Thr^{(P+2)}$ (Cld1), which makes the turn structure narrower and more rigid. In summary: Cld1 and Cld5 possess a narrower and more rigid turn region of the ECL2 than Cld3 and Cld4

to the slimmer ECL2 conformation, shows the strongest binding to $Cld5^{(P+1)}_{T151L}$ (Fig. 3b). Taken together, the turn conformation of ECL2 for Cld1, Cld3, Cld4 and Cld5 looks very similar, but it exhibits distinct slight conformational differences (Fig. S4), which are reflected in the divergent binding behavior and selectivity of cCPE versus these claudins.

cCPE: narrowing the claudin-binding pocket by S313H enhances Cld1- and enables Cld5-binding

Besides confirming that the triple mutant ($cCPE_{S305P/S307R/S313H}$) increases binding to Cld1 and that the single substitution S313H contributes most to this increased binding [29], we here demonstrate that the single substitution S313H alone enables binding to Cld5. This can be explained by our molecular interaction models. The small serine at position 313 of cCPE allows the interaction with the bulky ECL2 of Cld3 and Cld4 (Fig. 6a, b). The replacement of the serine side chain by the lager imidazole ring of histidine changes the shape and narrows the binding pocket of cCPE (Fig. 6c, d). Since Cld1 and Cld5 possess a slimmer shaped ECL2 than Cld3 and Cld4, the residue at P+2 ($Val^{152(P+2)}$ in Cld5 and $Thr^{153(P+2)}$ in Cld1) cannot interact properly with Ser^{313} at the peripheral rim of CPE's binding pocket (Fig. 6c, d), unlike the residue at P+2 in the ECL2 of Cld3 and Cld4 ($Val^{(P+2)}$ in both cases). Thus, a gap remains between the rim (dotted black line in cartoon, Fig. 6c) and the ECL2 of Cld1 and Cld5. S313H fills this particular space in the binding pocket. Consequently cCPE-constructs containing S313H fit much better to the slimmer conformation of the ECL2 of Cld1 and Cld5 compared to the bulkier turn of ECL2 of Cld3 and Cld4.

This suggested interaction with the particularly slim ECL2 turn is also supported by the lack of additional positive effects of S313H on binding to Cld1 and Cld5 constructs in which the conformation of the ECL2 is altered (e.g. $Cld1^{(P-1)}_{D150N}$, $Cld1^{(P+2)}_{T153V}$ and $Cld5^{(P-1)/(P+1)}_{D149N/T151L}$). However, additional contribution of an electrostatic effect by S313H on some claudins seems feasible, in particular for Cld1 and Cld7 both exhibiting Thr at position P+2.

The following modeling results can be seen as explanation for our findings that $cCPE_{S313H}$ does not show strong inhibition of binding to Cld3, −4, −6 and −9 and even exhibits slightly increased binding to Cld7 ($Thr^{(P+2)}$ like Cld1, see Fig. 1a). All the latter claudins are predicted to possess a wider ECL2 than Cld1 and Cld5, due to $Asn^{(P-1)}$, but since $Asn^{(P-1)}$ allows a more flexible turn compared to $Asp^{(P-1)}$ of Cld1 and Cld5; it is reasonable to assume that the side chain at P+2 might also be allowed in an intra-turn orientation in the ECL2 of Cld3, Cld4 and Cld6–Cld9 (Fig. 6). In addition, apart from $Asn^{(P-1)}$, all

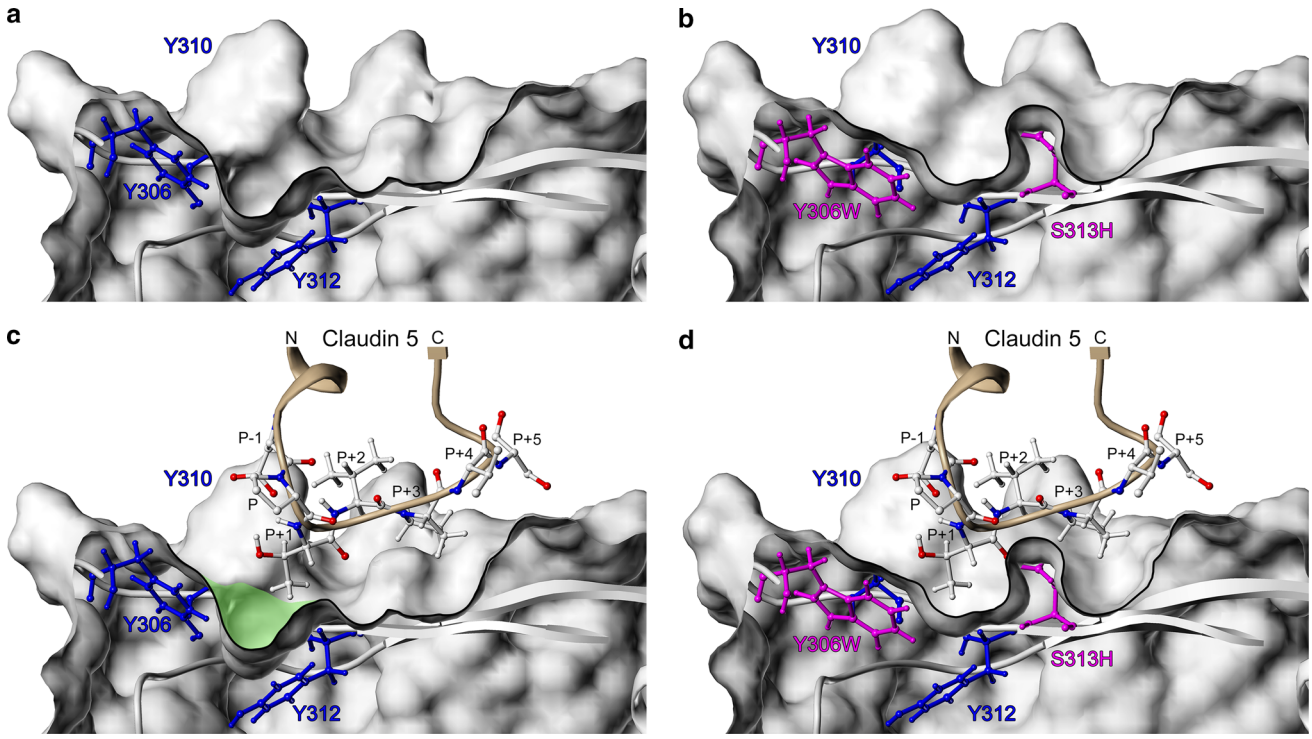

Fig. 7 Substitution Y306W downsizes the triple-Tyr pit, making it a better fit for Cld5. Cross section of the claudin-binding pocket of **a** $cCPE_{WT}$ and **b** $cCPE_{Y306W/S313H}$ and the interaction model of Cld5 with **c** $cCPE_{WT}$ and **d** $cCPE_{Y306W/S313H}$. cCPE is illustrated (*cartoon*, *white*) with the surface displayed (*white*) and the triple-Tyr pit defining residues in ball and stick (*blue*); substituted residues are depicted as ball and stick in *magenta*. ECL2 of Cld5 is shown in *beige*, with the residues of the turn region as ball and stick (*white*, C and H; blue, N; red, O). **c** $Thr^{(P+1)}$ of Cld5 is not able to fill the triple–Tyr pit of $cCPE_{WT}$ (highlighted in green), **d** by substituting Y^{306} with Trp the triple-Tyr pit was shrunken and closes the space to $Thr^{(P+1)}$ of Cld5

these claudins also possess a bulky hydrophobic residue at position P+1 which fills the triple-Tyr pit of the binding pocket (Figs. 1a, 2a, 6a) and thus contributes very strongly to CPE-binding.

cCPE: "pocket filler" mutant Y306 W downsizes the triple-Tyr pit and shifts specificity towards Cld5

The interaction between Cld3 or Cld4 with cCPE is processed by a knob and hole interaction of the bulky hydrophobic $Leu^{(P+1)}$ and triple-Tyr pit, respectively [9]. In Cld5, this bulky hydrophobic knob is missing; it contains instead very small residues at position P+1 ($Thr^{151(P+1)}$ in murine Cld5 or $Ser^{151(P+1)}$ in human Cld5) and it is thus a non-receptor claudin. To enable or enhance cCPE-binding of Cld5, the triple-Tyr pit had to be altered in such a way that it can compensate for the lack of bulky hydrophobic residues like Leu or Met at position P+1 of the ECL2 of Cld5. To achieve this, several putative "pit-filler" mutants were identified in silico, and then created and tested in vitro. We postulated that a true "pit-filler" mutant has to have increased binding to $Cld5_{WT}$, while showing decreased or no binding to claudins with a bulky hydrophobic residue at position P+1. Indeed, the introduction of the larger tryptophan side chain to replace tyrosine at position 306 of cCPE shows this effect when combined with S313H (Figs. 5a, b, 7). Compared to the binding pocket of $cCPE_{WT}$, the modeled binding pocket of $cCPE_{Y306W/S313H}$ shows clear downsizing of the triple-Tyr pit (Fig. 7a, b). In the interaction models of $cCPE_{WT}$ and $cCPE_{Y306W/S313H}$ with Cld5, substitution Y306W fills the void space (green in Fig. 7c) between $Thr^{(P+1)}$ of Cld5 and the triple-Tyr pit of cCPE (Fig. 7c, d). This explains why $cCPE_{Y306W/S313H}$ shows enhanced binding to $Cld5_{WT}$ compared to $cCPE_{WT}$ and $cCPE_{S313H}$, but decreased binding to all claudins which have a bulky hydrophobic residue at position P+1, such as in Cld1, Cld3, Cld4, $Cld5^{(P+1)}_{T151L}$, $Cld5^{(P-1/P+1)}_{D149N/T151L}$ and Cld6–Cld9 (Fig. 5a, b). The knob (P+1) of these claudins fails to interact with the closed hole (triple-Tyr pit of CPE). Thus, the effect of Y306W is due to an altered receptor site for the Thr/$Leu^{(P+1)}$ of Clds and of course always supported by other side chains such as the mutation S313H. Furthermore, $cCPE_{Y306W/S313H}$ shows enhanced binding to $Cld5_{WT}$, with a nanomolar K_d (33 ± 10 nM), which is of the same order of magnitude as the K_d of $cCPE_{WT}$ for the classic CPE

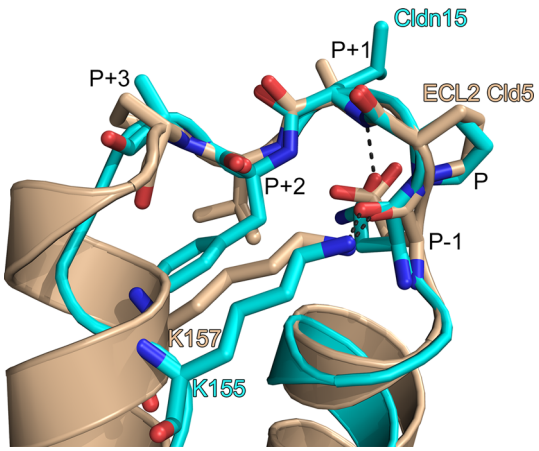

Fig. 8 Superposition of the interacting CPE interface for the initial Cld5-ECL2 model (*cartoon*, *beige*) and the crystal structure Cld15 (PDB ID: 4P79, *cartoon*, *cyan*) shows a high similarity. Residues of the turn region depicted as sticks (*white*, H; *blue*, N; *red*, O). Pairwise fit of the back bone atoms of the N-terminal helices and the turn region (Ile^{135}-Tyr^{151} in Cld15 and Leu^{136}-Val^{153} in Cld5) for the Cld5-ECL2 model (*beige*) and the Cld15 structure (*cyan*), demonstrates a high similarity and reveals an RMSD of 0.69 Å. The crystal structure of Cld15 confirms our initially postulated turn stabilizing interaction of Lys$^{157(P+7)}$ in Cld5 [1, 32] (Lys^{155} in Cld15) with the back bone carbonyl group of Asp$^{149(P-1)}$ (Asn^{148} in Cld15) as well as the involvement of the residue at position P−1 in the turn conformation

receptor claudins Cld3 and Cld4 ($K_d \approx 10$ nM) [7, 41]. cCPE$_{Y306W/S313H}$ also shows a strongly enhanced binding to the microvascular endothelial cEND cell line (Fig. 5d); these cells express Cld5 endogenously and are an in vitro model for the blood-brain barrier.

Claudin–15 structure confirms intramolecular stabilization of the ECL2 by Asn/Asp$^{(P-1)}$ and Lys$^{(P+7)}$

Recently two crystal structures of modified ECL2 peptides in complex with CPE were released (PDB ID: 3ZJ3 [42] and 4P5H [43]), which show opposing orientations of these peptides. However, the low resolutions of 3.37 Å and 3.38 Å do not allow explicit interpretation of H-bond interaction. Additionally and more importantly, a discrepancy concerning cCPE-binding to peptides versus binding to full-length claudins has already been observed since a Cld4 ECL2 peptide does not bind, whereas full-length Cld4 binds strongly [9, 30]. Thus, for the generation of homology models, the Cld15 structure (PDB ID: 4P79 [3]) with a resolution of 2.4 Å was used as a structural template for Cld1, –3, –4 and –5. This new crystal structure provides us with ideal means of assessing the performance of our claudin interaction models.

Our previous studies were based on initial ECL2 models with a helix-turn-helix motif [1, 6, 9, 30, 32]. We observed a remarkable structural agreement between these initial ECL2 models and the Cld15 structure in the N-terminal and especially in the central part, the turn region of ECL2, which is the interaction interface with cCPE (Fig. 8). This is demonstrated by the low RMSD values between Cld15 ECL2 (Ile^{135}-Tyr^{151}) to the initial Cld5 model (Leu^{136}-Val^{153}) = 0.69 Å (pairwise fitting of backbone atoms). The only difference between the initial ECL2 model and the Cld15 structure concerns the C-terminal part (Lys^{157}-Gly^{161} in Cld5 and the corresponding Lys^{155}-Gly^{159} in Cld15) for which we previously predicted a helical conformation, whereas the Cld15 structure shows a short beta strand that is interacting with the ECL1. However, this part is according to our results not directly participating in the essential CPE-binding region (Fig. 1a). Thus, the interacting interface of the initial ECL2 model of Cld5 to cCPE is nearly identical to the now solved crystal structure of Cld15.

More importantly, the crystal structure of Cld15 also indicates an involvement of Asn$^{(P-1)}$ in stabilization of the ECL2's turn structure, which is in line with our analysis of the impact of the Asn/Asp$^{(P-1)}$ difference in the ECL2 of claudins on binding of cCPE (Fig. 6). Furthermore, this crystal structure, also confirms our already previously [1, 32] postulated stabilization of the ECL2 turn by interaction of Lys$^{157(P+7)}$ with the back bone carbonyl group of Asp$^{149(P-1)}$ (Lys^{155} and Asn^{148} in Cld15) and the N-terminal helix of ECL2 (Fig. 8). Finally, the crystal structure confirms the main interacting turn conformation of our ECL2 models for claudins with cCPE.

In summary, we elucidated the molecular mechanism by which cCPE binds strongly to its receptor (Cld3), but only weakly to Cld1 and not at all to the non-receptor Cld5. By utilizing these insights, we generated a cCPE-variant with a specificity shifted away from the receptor claudins (e.g., Cld3, Cld4 and Cld6–Cld9) towards a non-receptor claudin (Cld5), by downsizing the binding pocket of cCPE, to complement the lack of a bulky hydrophobic residue in the ECL2 of Cld5. This newly developed cCPE-variant, with nanomolar affinity for Cld5, shows decreased binding to other claudins. Moreover, it demonstrated efficient binding to endogenous Cld5-expressing blood–brain barrier model cells, thus laying the foundation for high affinity tissue-specific claudin targeting. Therewith, we are able to provide the proof of principle that cCPE can be modified by multiple mutations in such a way that the specificity for claudins can be shifted even towards non-CPE receptor claudins. Apart from this new cCPE–claudin interaction pattern, differences in the structural properties of the ECL2 of claudins have been deduced and can be used to develop claudin subtype-specific binders as TJ modulators for tissue-specific drug delivery or for targeting cancer cells that overexpress claudin.

Acknowledgments This work was supported by Deutsche Forschungsgemeinschaft (DFG) grants KR 1273/3-2, PI 837/2-1 and by the Sonnenfeld Stiftung (PhD-scholarship for Miriam Eichner).

Conflict of interest The authors declare no conflict of interests.

References

1. Krause G, Winkler L, Mueller SL et al (2008) Structure and function of claudins. Biochim Biophys Acta 1778:631–645. doi:10.1016/j.bbamem.2007.10.018
2. Angelow S, Ahlstrom R, Yu ASL (2008) Biology of claudins. Am J Physiol Ren Physiol 295:F867–F876. doi:10.1152/ajprenal.90264.2008
3. Suzuki H, Nishizawa T, Tani K et al (2014) Crystal Structure of a claudin provides insight into the architecture of tight junctions. Science 344(80):304–307. doi:10.1126/science.1248571
4. McClane BA (2001) The complex interactions between Clostridium perfringens enterotoxin and epithelial tight junctions. Toxicon 39:1781–1791
5. Katahira J, Inoue N, Horiguchi Y et al (1997) Molecular cloning and functional characterization of the receptor for Clostridium perfringens enterotoxin. J Cell Biol 136:1239–1247
6. Veshnyakova A, Protze J, Rossa J et al (2010) On the interaction of Clostridium perfringens enterotoxin with claudins. Toxins (Basel) 2:1336–1356. doi:10.3390/toxins2061336
7. Sonoda N, Furuse M, Sasaki H et al (1999) Clostridium perfringens enterotoxin fragment removes specific claudins from tight junction strands: evidence for direct involvement of claudins in tight junction barrier. J Cell Biol 147:195–204
8. Kimura J, Abe H, Kamitani S et al (2010) Clostridium perfringens enterotoxin interacts with claudins via electrostatic attraction. J Biol Chem 285:401–408. doi:10.1074/jbc.M109.051417
9. Veshnyakova A, Piontek J, Protze J et al (2012) Mechanism of Clostridium perfringens enterotoxin interaction with claudin-3/-4 protein suggests structural modifications of the toxin to target specific claudins. J Biol Chem 287:1698–1708. doi:10.1074/jbc.M111.312165
10. Kitadokoro K, Nishimura K, Kamitani S et al (2011) Crystal structure of Clostridium perfringens enterotoxin displays features of beta-pore-forming toxins. J Biol Chem 286:19549–19555. doi:10.1074/jbc.M111.228478
11. Briggs DC, Naylor CE, Smedley JG 3rd et al (2011) Structure of the food-poisoning Clostridium perfringens enterotoxin reveals similarity to the aerolysin-like pore-forming toxins. J Mol Biol 413:138–149. doi:10.1016/j.jmb.2011.07.066
12. Van Itallie CM, Betts L, Smedley JG 3rd et al (2008) Structure of the claudin-binding domain of Clostridium perfringens enterotoxin. J Biol Chem 283:268–274. doi:10.1074/jbc.M708066200
13. Kokai-Kun JF, McClane BA (1997) Deletion analysis of the Clostridium perfringens enterotoxin. Infect Immun 65:1014–1022
14. Smedley JG 3rd, Uzal FA, McClane BA (2007) Identification of a prepore large-complex stage in the mechanism of action of Clostridium perfringens enterotoxin. Infect Immun 75:2381–2390. doi:10.1128/IAI.01737-06
15. Kondoh M, Takahashi A, Fujii M et al (2006) A novel strategy for a drug delivery system using a claudin modulator. Biol Pharm Bull 29:1783–1789
16. Takahashi A, Kondoh M, Suzuki H, Yagi K (2011) Claudin as a target for drug development. Curr Med Chem 18:1861–1865
17. Kondoh M, Masuyama A, Takahashi A et al (2005) A novel strategy for the enhancement of drug absorption using a claudin modulator. Mol Pharmacol 67:749–756. doi:10.1124/mol.104.008375
18. Kakutani H, Kondoh M, Fukasaka M et al (2010) Mucosal vaccination using claudin-4-targeting. Biomaterials 31:5463–5471. doi:10.1016/j.biomaterials.2010.03.047
19. Suzuki H, Kondoh M, Kakutani H et al (2012) The application of an alanine-substituted mutant of the C-terminal fragment of Clostridium perfringens enterotoxin as a mucosal vaccine in mice. Biomaterials 33:317–324. doi:10.1016/j.biomaterials.2011.09.048
20. Turksen K, Troy T-C (2011) Junctions gone bad: claudins and loss of the barrier in cancer. Biochim Biophys Acta 1816:73–79. doi:10.1016/j.bbcan.2011.04.001
21. Saeki R, Kondoh M, Kakutani H et al (2009) A novel tumor-targeted therapy using a claudin-4-targeting molecule. Mol Pharmacol 76:918–926. doi:10.1124/mol.109.058412
22. Kominsky SL, Tyler B, Sosnowski J et al (2007) Clostridium perfringens enterotoxin as a novel-targeted therapeutic for brain metastasis. Cancer Res 67:7977–7982. doi:10.1158/0008-5472.CAN-07-1314
23. Casagrande F, Cocco E, Bellone S et al (2011) Eradication of chemotherapy-resistant CD44+ human ovarian cancer stem cells in mice by intraperitoneal administration of Clostridium perfringens enterotoxin. Cancer 117:5519–5528. doi:10.1002/cncr.26215
24. Walther W, Petkov S, Kuvardina ON et al (2012) Novel Clostridium perfringens enterotoxin suicide gene therapy for selective treatment of claudin-3- and -4-overexpressing tumors. Gene Ther 19:494–503. doi:10.1038/gt.2011.136
25. Neesse A, Hahnenkamp A, Griesmann H et al (2013) Claudin-4-targeted optical imaging detects pancreatic cancer and its precursor lesions. Gut 62:1034–1043. doi:10.1136/gutjnl-2012-302577
26. Hsu L-W, Lee P-L, Chen C-T et al (2012) Elucidating the signaling mechanism of an epithelial tight-junction opening induced by chitosan. Biomaterials 33:6254–6263. doi:10.1016/j.biomaterials.2012.05.013
27. Krug SM, Amasheh M, Dittmann I et al (2013) Sodium caprate as an enhancer of macromolecule permeation across tricellular tight junctions of intestinal cells. Biomaterials 34:275–282. doi:10.1016/j.biomaterials.2012.09.051
28. Tscheik C, Blasig IE, Winkler L (2013) Trends in drug delivery through tissue barriers containing tight junctions. Tissue barriers 1:e24565. doi:10.4161/tisb.24565
29. Takahashi A, Saito Y, Kondoh M et al (2012) Creation and biochemical analysis of a broad-specific claudin binder. Biomaterials 33:3464–3474. doi:10.1016/j.biomaterials.2012.01.017
30. Winkler L, Gehring C, Wenzel A et al (2009) Molecular determinants of the interaction between Clostridium perfringens enterotoxin fragments and claudin-3. J Biol Chem 284:18863–18872. doi:10.1074/jbc.M109.008623
31. Blasig IE, Winkler L, Lassowski B et al (2006) On the self-association potential of transmembrane tight junction proteins. Cell Mol Life Sci 63:505–514. doi:10.1007/s00018-005-5472-x
32. Piontek J, Winkler L, Wolburg H et al (2008) Formation of tight junction: determinants of homophilic interaction between classic claudins. FASEB J 22:146–158. doi:10.1096/fj.07-8319com
33. Piontek J, Fritzsche S, Cording J et al (2011) Elucidating the principles of the molecular organization of heteropolymeric tight junction strands. Cell Mol Life Sci 68:3903–3918. doi:10.1007/s00018-011-0680-z
34. Rossa J, Ploeger C, Vorreiter F et al (2014) Claudin-3 and Claudin-5 protein folding and assembly into the tight junction are controlled by non-conserved residues in the transmembrane 3 (TM3) and extracellular loop 2 (ECL2) segments. J Biol Chem 289:7641–7653. doi:10.1074/jbc.M113.531012

35. Van den Ent F, Löwe J (2006) RF cloning: a restriction-free method for inserting target genes into plasmids. J Biochem Biophys Methods 67:67–74. doi:10.1016/j.jbbm.2005.12.008
36. Kleinschnitz C, Blecharz K, Kahles T et al (2011) Glucocorticoid insensitivity at the hypoxic blood-brain barrier can be reversed by inhibition of the proteasome. Stroke 42:1081–1089. doi:10.1161/STROKEAHA.110.592238
37. Baltzegar DA, Reading BJ, Brune ES, Borski RJ (2013) Phylogenetic revision of the claudin gene family. Mar Genomics 11:17–26. doi:10.1016/j.margen.2013.05.001
38. Krause G, Winkler L, Piehl C et al (2009) Structure and function of extracellular claudin domains. Ann N Y Acad Sci 1165:34–43. doi:10.1111/j.1749-6632.2009.04057.x
39. Förster C, Silwedel C, Golenhofen N et al (2005) Occludin as direct target for glucocorticoid-induced improvement of blood-brain barrier properties in a murine in vitro system. J Physiol 565:475–486. doi:10.1113/jphysiol.2005.084038
40. Blecharz KG, Haghikia A, Stasiolek M et al (2010) Glucocorticoid effects on endothelial barrier function in the murine brain endothelial cell line cEND incubated with sera from patients with multiple sclerosis. Mult Scler 16:293–302. doi:10.1177/1352458509358189
41. Fujita K, Katahira J, Horiguchi Y et al (2000) Clostridium perfringens enterotoxin binds to the second extracellular loop of claudin-3, a tight junction integral membrane protein. FEBS Lett 476:258–261
42. Yelland TS, Naylor CE, Savva CG, et al. (2014) Structure of Clostridium perfringens enterotoxin with a peptide derived from a modified version of ECL-2 of Claudin 2. PDB ID: 3ZJ3, doi:10.2210/pdb3zj3/pdb
43. Yelland TS, Naylor CE, Bagoban T et al (2014) Structure of a C. perfringens enterotoxin mutant in complex with a Modified Claudin-2 Extracellular Loop 2. J Mol Biol. doi:10.1016/j.jmb.2014.07.001